# Critical behavior of the quantum Stirling heat engine

Yuan-Sheng Wang,[1,2] Man-Hong Yung,[3,4,5,6] Dazhi Xu,[7,*] Maoxin Liu,[1,†] and Xiaosong Chen[1,‡]

[1]*School of Systems Science, Beijing Normal University, Beijing 100875, China*
[2]*Lanzhou Center for Theoretic Physics, Lanzhou University, Lanzhou, Gansu 730000, China*
[3]*Department of Physics, Southern University of Science and Technology, Shenzhen 518055, China*
[4]*Shenzhen Institute for Quantum Science and Engineering, Southern University of Science and Technology, Shenzhen 518055, China*
[5]*Guangdong Provincial Key Laboratory of Quantum Science and Engineering, Southern University of Science and Technology, Shenzhen 518055, China*
[6]*Shenzhen Key Laboratory of Quantum Science and Engineering, Southern University of Science and Technology, Shenzhen 518055, China*
[7]*Center for Quantum Technology Research and Key Laboratory of Advanced Optoelectronic Quantum Architecture and Measurements (MOE), School of Physics, Beijing Institute of Technology, Beijing 100081, China*

(Received 3 July 2023; accepted 12 January 2024; published 8 February 2024)

We investigate the performance of a Stirling cycle with a working substance (WS) modeled as the quantum Rabi model (QRM), exploring the impact of criticality on its efficiency. Our findings indicate that the criticality of the QRM has a positive effect on improving the efficiency of the Stirling cycle when the WS parameters are in the normal phase. Furthermore, we observe that the Carnot efficiency is asymptotically achievable as the WS parameter approaches the critical point, even when both temperatures of the cold and hot reservoirs are finite. Additionally, we derive the critical behavior for the efficiency of the Stirling cycle, demonstrating how the efficiency asymptotically approaches the Carnot efficiency as the WS parameter approaches the critical point. Our work deepens the understanding of the impact of criticality on the performance of a Stirling heat engine.

DOI: 10.1103/PhysRevA.109.022208

## I. INTRODUCTION

Recently, there has been a growing interest in exploring the application of thermodynamics in the quantum regime, facilitated by advancements in experimental control over various quantum systems [1,2]. While classical thermodynamics traditionally focused on large systems governed by classical physics, the emergence of quantum heat engines (QHEs) has provided a valuable platform for testing the principles of thermodynamics in the quantum realm. QHEs operate utilizing quantum effects in either the reservoir or the working substance (WS) to convert heat into work through a thermodynamic cycle. Extensive research in the field of QHEs [3–7] has demonstrated that quantum effects, such as quantum coherence [8–12], quantum correlation [13,14], and energy quantization [15], can be harnessed to enhance their performance.

QHEs have been implemented in various experimental platforms, including cold atoms [16,17], trapped ions [18–20], optomechanical oscillators [21–25], quantum dots [26–29], spins [9,14,30–34], and superconducting circuits [35–37], among others. Recent studies suggest that the criticality may substantially impact the performance of QHEs [38–54], with some research indicating that criticality could offer advantages in improving efficiency. For instance, by modeling the WS of a Stirling cycle as a Lipkin-Meshkov-Glick model and exploiting its criticality, it is possible to approach the Carnot efficiency in the low-temperature limit [38]. In Ref. [39] it has been demonstrated that criticality can enable quantum Otto engines to approach Carnot efficiency without sacrificing power. Another study [40] proposed a thermodynamic cycle with two interaction-driven Stokes using a one-dimensional ultracold gas as the WS, revealing that the average work per particle approaches a maximum at the critical point.

However, it is not yet fully understood how universality at the critical point impacts the efficiency of QHEs. Resolving this issue requires determining the asymptotic behavior of a quantum heat engine as its parameters approach the critical point. To this end, it would be beneficial to consider a model with an analytical solution and a phase transition that can be easily observed through experiments. Recent research has demonstrated that a quantum phase transition (QPT) can occur in a system of only two constituents: a two-level atom and a bosonic mode [55,56]. This system, described by the quantum Rabi model (QRM) and with an analytical solution, has been experimentally observed to exhibit QPT using trapped ions in a Pauli trap [57]. QHEs with WSs described by the QRM or generalized QRM have been explored in several research works [58,59].

In this paper we investigate the critical behavior of Stirling engine efficiency based on WSs modeled as the QRM. Firstly,

*dzxu@bit.edu.cn
†mxliu@bnu.edu.cn
‡chenxs@bnu.edu.cn

 ©2024 American Physical Society

we analyze whether criticality is beneficial for improving the efficiency of such QHE by using the analytical solution of the QRM. Furthermore, we derive the asymptotic behavior of efficiency as a control parameter approaches the critical point, which illustrates a dependence on the critical exponent. Additionally, we present numerical verifications that support our findings. This result improves our understanding of heat engines utilizing criticality. Furthermore, we observe an extension of prior knowledge, where a Stirling cycle can approach the Carnot efficiency at the critical point at finite temperature.

This paper is organized as follows. Section II introduces the quantum Stirling heat engine and the QRM. In Sec. III we explore the influence of criticality on the efficiency of a quantum Stirling heat engine, including a discussion of the efficiency's asymptotic behavior in the vicinity of the critical point. In Sec. IV numerical results are presented to support the findings introduced in Sec. III. Lastly, Sec. V provides a summary of the key findings.

## II. THE QUANTUM STIRLING HEAT ENGINE

### A. The quantum Rabi model

First we introduce the QRM, which is considered as the WS in this work. The QRM Hamiltonian can be expressed as (for simplicity, we set $\hbar = 1$ here and after)

$$H_{\text{Rabi}} = \omega_0 a^\dagger a + \frac{\Omega}{2}\sigma_z - \lambda\left(a + a^\dagger\right)\sigma_x, \tag{1}$$

where $\sigma_{x,z}$ are Pauli matrices for a two-level system, $a$ ($a^\dagger$) is an annihilation (creation) operator for a cavity field, and $\lambda$ is the coupling strength. Introducing a dimensionless coupling constant $g = 2\lambda/\sqrt{\omega_0\Omega}$, in the limit $\xi \equiv \Omega/\omega_0 \to \infty$, the Rabi model undergoes a second-order QPT at the critical point $g = g_C \equiv 1$ [55], which can be illustrated in a pedagogic way [60]. The position and momentum operators $x = (a^\dagger + a)/\sqrt{2\xi}$, and $p = i\sqrt{\xi}(a^\dagger - a)/\sqrt{2}$. The Hamiltonian in Eq. (1) becomes $H'_{\text{Rabi}} = H_{\text{Rabi}}/\Omega$, namely,

$$H'_{\text{Rabi}} = \frac{\sigma_z}{2} + \frac{p^2}{2\xi^2} + \frac{g^2\sigma_z + 1}{2}x^2 - \frac{g^4}{4}\sigma_z x^4. \tag{2}$$

Taking the limit $\xi \to \infty$, the term of $p^2/(2\xi^2)$ should be neglected and the low-energy effective potential is

$$\varepsilon_0(x) = -\frac{1}{2} + \frac{1-g^2}{2}x^2 + \frac{g^4}{4}x^4 + \cdots, \tag{3}$$

which has the Landau form. One readily concludes that if $g < g_C$, $\varepsilon_0(x)$ has one minimum at $x = 0$, and if $g > g_C$, there will be two nonzero minima, indicating a symmetry-breaking phase. When $g < g_C$, there is no photon number expectation indicating a normal phase, and when $g > g_C$, a nonzero photon number expectation arises, which is known as the superradiant phase.

Even though the $H'_{\text{Rabi}}$ reveals the mechanism of phase transition in the quantum model, it becomes classical by dropping the $p^2$ term. To obtain the energy spectra of the QRM in the vicinity of the critical point, we apply an alternative way to introduce the effective Hamiltonian following Ref. [55]. In the normal phase, by applying a unitary transformation the effective Hamiltonian can be obtained as

$$H_{\text{eff}} = \Lambda^\dagger H_{\text{Rabi}}\Lambda, \tag{4}$$

where

$$\Lambda = \exp\left[\frac{\lambda}{\omega}(a + a^\dagger)(\sigma_+ - \sigma_-)\right]. \tag{5}$$

The transformed Hamiltonian (4) decouples the spin subspace $\mathcal{H}_\downarrow$ and $\mathcal{H}_\uparrow$, and by projecting it onto $\mathcal{H}_\downarrow$, one gets the low-energy effective Hamiltonian of the QRM in the normal phase:

$$H_{\text{np}} = \omega_0 a^\dagger a - \frac{\omega_0 g^2}{4}(a + a^\dagger)^2 - \frac{\Omega}{2}. \tag{6}$$

Diagonalizing this Hamiltonian into $H_{\text{np}} = \varepsilon_{\text{np}} b^\dagger b - \Omega/2$, with the excitation energy

$$\varepsilon_{\text{np}} = \omega_0\sqrt{1 - g^2}. \tag{7}$$

$\varepsilon_{\text{np}}$ is real only for $g \leqslant g_C$ and vanishes at $g = g_C$. In the superradiant phase, where $g > 1$, the low-energy effective Hamiltonian reads

$$H_{\text{sp}} = \omega_0 a^\dagger a - \frac{\omega_0}{4g^4}(a + a^\dagger)^2 - \frac{\Omega}{4}(g^2 + g^{-2}), \tag{8}$$

which is in a displaced frame of the bosonic mode. Due to its strong coupling to the bosonic mode, the qubit ground state rotates toward the $x$ axis. The Hamiltonian (8) has a similar form as (6), which can be diagonalized similarly, resulting in $H_{\text{sp}} = \varepsilon_{\text{sp}} b^\dagger b - \Omega(g^2 + g^{-2})/4$. The energy spectra in the superradiant phase are twice degenerate with excitation energy

$$\varepsilon_{\text{sp}} = \omega_0\sqrt{1 - g^{-4}}, \tag{9}$$

which is real for $g > g_C$.

In this work we mainly discuss the thermodynamics of the QRM in the normal phase and require all the thermodynamic processes to be quasistatic. The equilibrium state of the QRM can be described by the Gibbs state $\rho = \exp(-H_{\text{np}}/T)/\mathcal{Z}$, where $\mathcal{Z} = \text{Tr}[\exp(-H_{\text{np}}/T)]$ is the partition function and $T$ is the temperature (we set the Boltzmann constant $k_B = 1$ here and after). With straightforward calculation, we can obtain the internal energy $U = T^2\partial \ln \mathcal{Z}/\partial T$ and the entropy $S = U/T + \ln \mathcal{Z}$ as

$$U = \frac{\varepsilon_{\text{np}}}{\exp(\varepsilon_{\text{np}}/T) - 1} - \frac{\Omega}{2}, \tag{10}$$

$$S = \frac{\varepsilon_{\text{np}}/T}{\exp(\varepsilon_{\text{np}}/T) - 1} - \ln[1 - \exp(-\varepsilon_{\text{np}}/T)]. \tag{11}$$

### B. The quantum Stirling cycle

The QRM Stirling heat engine cycle comprises four quasistatic thermodynamic processes, as illustrated in the Fig. 1. This cycle involves two isothermal processes, A → B and C → D, and two isochoric processes, B → C and D → A. In the isothermal process A → B (C → D), the control parameter $g$ increases from $g_1$ to $g_2$ (decreases from $g_2$ to $g_1$) while maintaining thermal contact between the system and a heat bath at high (low) temperature $T_{\text{h}}$ ($T_{\text{c}}$). In practical terms, the QRM could be realized using a single atom in a single-mode cavity field, and the heat bath could be modeled by the environmental multimode electromagnetic fields. To ensure that the working substance remains in thermal equilibrium

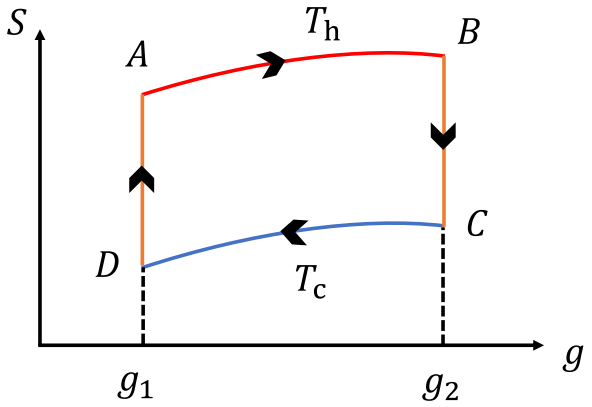


FIG. 1. Entropy-coupling diagram ($S-g$) of the Stirling cycle (clockwise or anticlockwise, depending on the work output), which consists of two isothermal processes and two isochoric processes. Here $g$ is the only tunable parameter in completing the Stirling cycle; $g_1$ and $g_2$ are the corresponding parameters in the two isochoric processes D $\to$ A and B $\to$ C, respectively; and $T_h$ and $T_c$ are the corresponding temperatures of hot (A $\to$ B) and cold (C $\to$ D) isothermal processes, respectively.

with the heat bath, we assume that the change of eigenenergy spectra is much slower than the system relaxation. The details of the system-bath coupling do not affect the conclusions of this work. During the isochoric processes, the control parameter $g$ is fixed at $g_2$ for B $\to$ C and $g_1$ for D $\to$ A. To ensure that the isochoric process proceeds quasistatically, we assume that the system is in contact with a heat bath that slowly changes its temperature from $T_h$ to $T_c$ for B $\to$ C and from $T_c$ to $T_h$ for D $\to$ A.

In this study we adopt a convention where the work done to the outside and heat absorbed by the system are considered positive, and vice versa. We define heat and entropy variation during the process X $\to$ Y as $Q_{XY}$ and $S_{XY}$, respectively, where X(Y) represents the state of A, B, C, or D. As entropy is a state function, we have $S_{XY} = S_Y - S_X$. In one cycle, the total heat absorbed by the quantum Stirling heat engine reads

$$Q_{in} = Q_{AB} + Q_{DA}, \tag{12}$$

and the total output work is

$$W = Q_{AB} + Q_{BC} + Q_{CD} + Q_{DA}. \tag{13}$$

In the quasistatic isothermal processes, the heat exchanges can be calculated by $Q_{AB} = T_h S_{AB}$ and $Q_{CD} = T_c S_{CD}$, respectively. While in the isochoric processes, because the work done is zero, the heat exchanges can be obtained from the variation of internal energy, $Q_{DA} = U_A - U_D$ and $Q_{BC} = U_C - U_B$.

Therefore the efficiency of the quantum Stirling heat engine defined by $\eta = W/Q_{in}$ can be expressed as

$$\eta = \frac{\eta_C + \Sigma_1 + \Sigma_2}{1 + \Sigma_2}, \tag{14}$$

where $\eta_C = 1 - T_c/T_h$ is the Carnot efficiency and

$$\Sigma_1 = [Q_{BC} - T_c(S_{DA} + S_{BC})]/Q_{AB}, \tag{15}$$

$$\Sigma_2 = Q_{DA}/Q_{AB}. \tag{16}$$

We emphasize that the derivation of Eq. (14) is independent of the WS.

The Carnot cycle comprises two isothermal processes and two adiabatic processes, with its efficiency $\eta_C$ establishing an upper limit for the efficiency of any classical thermodynamic cycle. The Stirling cycle is obtained by substituting the two adiabatic processes in the Carnot cycle with two isochoric processes, and its efficiency is given in Eq. (14). The difference between Eq. (14) and the Carnot efficiency stems from $\Sigma_1$ and $\Sigma_2$, which arises due to the irreversibility of the isochoric processes. In the subsequent section we will illustrate that by employing the criticality of the QRM; the difference between the Stirling efficiency given in Eq. (14) and the Carnot efficiency can be asymptotically eliminated.

## III. THE CRITICAL BEHAVIOR OF QRM STIRLING ENGINE

### A. Heat engine efficiency near critical point

In this section we consider a Stirling cycle with the WS modeled as the QRM, and we employ the $g$ as the only tunable parameter. We will demonstrate that when the thermodynamic cycle introduced in the previous section satisfies the condition $g_1 < g_2 \to g_C$, the corresponding efficiency approaches the Carnot limit. To validate this conclusion, we first show that as $g_2$ approaches the critical point $g_C$, both $\Sigma_1$ and $\Sigma_2$, defined in Eqs. (15) and (16), converge to zero. To demonstrate this we will prove that the quantities in the numerators ($Q_{DA}$, $Q_{BC}$, $S_{DA}$, and $S_{BC}$) are finite. More importantly, we will subsequently show that $Q_{AB}$ in the denominator diverges as $g_2$ approaches $g_C$.

The output work is zero in the quantum isochoric process at $g_1$. As a result, the heat absorbed from the bath $Q_{DA}$ equals the change of internal energy, which can be calculated by

$$Q_{DA} = \int_{T_c}^{T_h} \frac{\partial U(T, g_1)}{\partial T} dT \equiv \int_{T_c}^{T_h} \mathcal{C}[\varepsilon_{np}(g_1)/T] dT. \tag{17}$$

Here, we defined the isochoric capacity $\mathcal{C}[\varepsilon_{np}(g_1)/T]$, which can be expressed by the function $\mathcal{C}(x) = (x/2)^2 \mathrm{csch}^2(x/2)$ (see Appendix A for details). When $x \in (0, \infty)$, it can be proved that $\mathcal{C}(x)$ is a finite monotonic decreasing function, with limits

$$\lim_{x\to 0} \mathcal{C}(x) = 1 \text{ and } \lim_{x\to\infty} \mathcal{C}(x) = 0. \tag{18}$$

With the above properties of $\mathcal{C}(x)$, it is straightforward to show that $Q_{DA}$ is finite with bounds

$$0 < Q_{DA} < (T_h - T_c)\mathcal{C}[\varepsilon_{np}(g_1)/T_h]. \tag{19}$$

By the same logic, the heat release $Q_{BC}$ in the isochoric process at $g_2$ is bounded by

$$-(T_h - T_c)\mathcal{C}[\varepsilon_{np}(g_2)/T_h] < Q_{BC} < 0. \tag{20}$$

The change of entropy during the isochoric process D $\to$ A can be written as

$$S_{DA} = \int_{T_c}^{T_h} \frac{\partial S(T, g_1)}{\partial T} dT = \int_{T_c}^{T_h} \frac{1}{T} \mathcal{C}[\varepsilon_{np}(g_1)/T] dT, \tag{21}$$

where we have used Eqs. (10) and (11) in deriving the last step. According to the monotonicity of $\mathcal{C}(x)$, it can be found

that

$$0 < S_{\rm DA} < \frac{T_{\rm h} - T_{\rm c}}{T_{\rm c}} \mathcal{C}[\varepsilon_{\rm np}(g_1)/T_{\rm h}]. \tag{22}$$

Similarly, we can also obtain

$$-\frac{T_{\rm h} - T_{\rm c}}{T_{\rm c}} \mathcal{C}[\varepsilon_{\rm np}(g_2)/T_{\rm h}] < S_{\rm BC} < 0. \tag{23}$$

Now we have shown that the numerators of $\Sigma_1$ and $\Sigma_2$ are finite for nonzero Carnot efficiency ($T_{\rm h} \neq T_{\rm c}$). Whether $\eta$ can approach $\eta_C$ depends on whether $Q_{\rm AB} = T_{\rm h} S_{\rm AB}$ is divergent or not. In the isochoric process B $\to$ C, the energy spectra tend to degenerate, $\varepsilon_{\rm np}(g_2) \to 0$ when $g_2 \to g_C$. According to Eq. (11), the entropy $S_{\rm B}$ can be approximated as

$$S_{\rm B} \approx -\ln[\varepsilon_{\rm np}(g_2)/T_{\rm h}] \tag{24}$$

when $\varepsilon_{\rm np}(g_2)/T_{\rm h} \ll 1$. Hence, the entropy $S_{\rm B}$ is divergent near the critical point (note that $S_{\rm C}$ is also divergent, but $S_{\rm BC}$ is finite due to the finite capacity). On the other hand, in the isochoric process D $\to$ A, the entropy $S_{\rm A}$ is finite because the energy gap $\varepsilon_{\rm np}(g_1)/T_{\rm h}$ is finite. As a result,

$$\lim_{g_2 \to g_C} Q_{\rm AB} \equiv T_{\rm h}(S_{\rm B} - S_{\rm A}) \to +\infty. \tag{25}$$

The above facts imply

$$\lim_{g_2 \to g_C} \Sigma_1 = \Sigma_2 = 0. \tag{26}$$

Therefore we have proved that under the condition $(g_1 <) g_2 \to g_C$, the efficiency of the QRM Stirling engine can approach the Carnot limit.

It must be emphasized that the aforementioned conclusion is specifically applicable to finite temperatures. When approaching the critical point in the low-temperature limit, two different orders of the limits, $\lim_{T\to 0} \lim_{g_2 \to g_C}$ and $\lim_{g_2 \to g_C} \lim_{T \to 0}$, are not equivalent. The former one is proper in the low-temperature limit. As in this case, the population will be uniformly distributed over all the degenerate states, resulting in the divergence of the entropy, i.e., $S_{\rm B},\ S_{\rm D} \to \infty$. Moreover, we also require $\varepsilon_{\rm np}/T$ to be finite even when $T \to 0$. Therefore, the heat engine in the low-temperature limit has the same thermodynamic behavior as the finite-temperature case. On the other hand, if the order $\lim_{g_2 \to g_C} \lim_{T \to 0}$ is adopted, all the populations will leave in the nondegenerate ground state when the energy gap $\varepsilon_{\rm np}$ is finite, resulting in a zero entropy in the low-temperature limit.

It is noteworthy that in this work a discussion of the high-temperature limit is precluded due to the following rationale: To address the critical behavior, we use the low-energy effective Hamiltonian of the QRM. Thus, thermodynamics involves high-energy spectra in the high-temperature limit, and our approach will lead to inaccurate results.

The high efficiency of the QRM Stirling heat engine relies on the divergence of the entropy variation $S_{\rm AB}$ during the isothermal process, which is a consequence of the energy spectra degenerating at the critical point. Despite the irreversibility of the two isochoric processes, the entropy production during these processes can be considered negligible in comparison to $S_{\rm AB}$. It is noteworthy that the classical Stirling heat engine can also approach the Carnot limit, but the mechanism differs significantly from its quantum counterpart discussed here. In the classical Stirling cycle, heat exchanges in the two isochoric processes are facilitated by a component called a regenerator [61], ensuring that the heat absorbed and released from the bath precisely cancel each other. Consequently, the classical Stirling heat engine can approach the Carnot efficiency. However, in our quantum Stirling heat engine case, achieving Carnot efficiency through the regenerator is impossible due to the different heat capacities at $g_1$ and $g_2$. Therefore the heat exchanges in the two isochoric processes no longer cancel each other.

In practice, it is crucial to emphasize that reaching or crossing the critical point via a quantum isothermal process in finite time is unattainable in the infinity $\xi$ limit. Instead, our focus is on the critical behavior of a quasistatic thermodynamic cycle by tuning $g_2$ asymptotically approaching $g_C$ without referring to the relaxation dynamics of the QRM. In such a quasistatic cycle, once the control protocol of $g$ is fixed, the QRM can only serve as a heat engine ($Q_{\rm in} > 0$, $Q_{\rm out} < 0$, and $W > 0$). This conclusion is based on the following reasons: Eqs. (20) and (25) imply $Q_{\rm in} = Q_{\rm DA} + Q_{\rm AB} > 0$. By the same approach, it can be demonstrated that $Q_{\rm out} = Q_{\rm BC} + Q_{\rm CD} < 0$. Moreover, the efficiency is positive as $\eta \to \eta_C$, and then $W = \eta Q_{\rm in}$ is also positive. However, in the case of a finite-time cycle, the quantum heat engine could also operate in other modes, as suggested in Refs. [57,62].

At the end of this section we will establish that the efficiency converges to the Carnot efficiency as $g_2$ crosses the critical point in the low-temperature limit. This assertion is made under the assumption that $T_{\rm c}/T_{\rm h}$ is a finite constant. In the low-temperature limit, the system resides in the ground state as $T_{\rm h} \to 0$. In the normal phase, the ground state is nondegenerate, resulting in $\lim_{T_{\rm h}\to 0} S_{\rm A} = S_{\rm D} \to 0$. However, when $g_2 > g_C$, the ground state exhibits a twofold degeneracy (as mentioned in Sec. II A). In the low-temperature limit, the system is evenly distributed between these two degenerate ground states, leading to $\lim_{T_{\rm h}\to 0} S_{\rm AB} = S_{\rm B} \to \ln 2$. Next, we aim to demonstrate that $\lim_{T_{\rm h}\to 0} Q_{\rm BC}/Q_{\rm AB} \to 0$. In the case of $g_2 > g_C$, the stroke B $\to$ C operates in the superradiant phase, and we can derive two inequalities similar to Eqs. (20) and (23) in the normal phase, by only substituting the excitation energy in the normal phase $\varepsilon_{\rm np}$ with the one in the superradiant phase $\varepsilon_{\rm sp}$ (see Appendix A for details):

$$-(T_{\rm h} - T_{\rm c})\mathcal{C}[\varepsilon_{\rm sp}(g_2)/T_{\rm h}] < Q_{\rm BC} < 0, \tag{27}$$

$$-\frac{T_{\rm h} - T_{\rm c}}{T_{\rm c}} \mathcal{C}[\varepsilon_{\rm sp}(g_2)/T_{\rm h}] < S_{\rm BC} < 0. \tag{28}$$

Furthermore, by dividing the inequality (27) by $Q_{\rm AB}$ and using the result $\lim_{T\to 0} \mathcal{C}(\varepsilon_{\rm sp}/T) \to 0$ of Eq. (18), we have

$$\lim_{T_{\rm h}\to 0} Q_{\rm BC}/Q_{\rm AB} \to 0. \tag{29}$$

In the same manner, it can be proven that the following ratios $Q_{\rm DA}/Q_{\rm AB}$, $S_{\rm DA}/S_{\rm AB}$, $S_{\rm BC}/S_{\rm AB}$ all approach to zero when $T_{\rm h} \to 0$. Combining these results with Eqs. (14), (15), and (16), we arrive at $\lim_{T_{\rm h}\to 0} \eta \to \eta_C$. In summary, for a Stirling heat engine with the WS modeled as the QRM, in the limit as $\xi \to \infty$, when $g_1 < g_C$ and $g_2 > g_C$, the efficiency tends towards the Carnot efficiency in the low-temperature limit.

### B. The critical behavior of the efficiency

In this section we will discuss the critical behavior of efficiency, focusing on how $\eta$ approaches $\eta_C$ as $g_2 \to g_C$. When $g_2$ is sufficiently close to $g_C$, from Eq. (26) we see that $\Sigma_1, \Sigma_2 \ll 1$. To the first order of $\Sigma_1$ and $\Sigma_2$, Eq. (14) can be approximated as

$$\eta - \eta_C \approx \Sigma_1 + (1-\eta_C)\Sigma_2 \approx -\frac{\alpha}{S_{\rm AB}}, \tag{30}$$

where the term

$$\alpha \equiv (1-\eta_C)\left(\frac{Q_{\rm DA}}{T_{\rm h}} + \frac{Q_{\rm BC}}{T_{\rm c}} - S_{\rm DA} - S_{\rm BC}\right) \tag{31}$$

is finite according to Eqs. (19), (20), (22), and (23). On the other hand, we can prove

$$\lim_{|g_2-g_C|\to 0} S_{\rm AB} \to -\ln[\varepsilon_{\rm np}(g_2)/T_{\rm h}], \tag{32}$$

based on the fact of Eq. (24) and $S_{\rm B}$ is finite. Therefore, considering the normal phase energy spectral $\varepsilon_{\rm np} = \omega_0\sqrt{1-g^2}$ given by Eq. (7), we obtain the critical behavior of the heat engine efficiency as

$$\lim_{|g_2-g_C|\to 0} \eta_C - \eta \to \frac{\alpha}{\ln[\varepsilon_{\rm np}(g_2)/T_{\rm h}]} \propto \frac{\alpha}{\ln{(g_C-g_2)^{z\nu}}}, \tag{33}$$

where $z\nu = 1/2$ is the dynamical critical exponent. We can readily further conclude that Eq. (33) is valid for any WSs with homogeneous energy-level spacing $\varepsilon_{\rm np(sp)}(g) \propto |g_C - g|^{z\nu}$ in the vicinity of the critical point and undergoes a thermodynamic cycle depicted in Sec. II. From Eq. (33) we readily know that the efficiency $\eta$ approaches the Carnot efficiency $\eta_C$ when the $g_2 \to g_C$, which means that by approaching the critical coupling point, the efficiency of the heat engine can be greatly improved by approaching the Carnot efficiency. Furthermore, Eq. (33) describes the asymptotic behavior of a quantum heat engine when approaching the critical point and illustrates how the efficiency depends on the critical exponent. This asymptotic behavior is characterized by a logarithmic divergence in the denominator of Eq. (33).

## IV. NUMERICAL RESULTS

This section presents numerical demonstrations to support the conclusions drawn in the previous section. In deriving the numerical results, we first perform numerical diagonalization on the Hamiltonian of the QRM in Eq. (1) (see Appendix B for details). Denoting the eigenvalues as $\{E_k|k = 1, 2, \ldots, N\}$, for a Gibbs state of temperature $T$, the $k$th energy population reads $P_k(T, g) = \exp[-E_k(g)/T]/\mathcal{Z}(T, g)$, and the partition function is given by $\mathcal{Z}(T, g) = \sum_l \exp[-E_l(g)/T]$. The entropy and internal energy are computed by the following expressions:

$$S(T, g) = -\sum_k P_k(T, g)\ln P_k(T, g), \tag{34}$$

$$U(T, g) = -\sum_k P_k(T, g)E_k(g). \tag{35}$$

The entropies (internal energies) $S_i(U_i)$, $i$ = A,B,C,D can be calculated with the associated $T$ and $g$ according to the Stirling protocol shown in Fig. 1. The heat exchanges during the four strokes in Eqs. (12) and (13) are $Q_{\rm AB} = T_{\rm h}S_{\rm AB}$, $Q_{\rm CD} = T_{\rm c}S_{\rm CD}$, $Q_{\rm BC} = U_{\rm C} - U_{\rm B}$, $Q_{\rm DA} = U_{\rm A} - U_{\rm D}$. Further, we can obtain $Q_{\rm in}$ and $W$ and the efficiency $\eta = W/Q_{\rm in}$. In the simulation, we chose $g_1 = 0.2$, $\omega_0 = 2\pi\times 0.2$ kHz, $\Omega = 2\pi\times(20, 40, 80)$ kHz, $\xi = 100,\ 200,\ 400$, and $0.2 \leqslant g_2 \leqslant 1.8$. Those parameters are roughly consistent with those in a recent theoretic proposal [63] and experimental realization [64] of observing QRM QPT in a trapped-ion system. It should be noted that although reaching or crossing the critical point via a quantum isothermal process in finite time is unattainable in the infinite $\xi$ limit, it is allowed in the finite-$\xi$ case, as we considered in our numerical calculations.

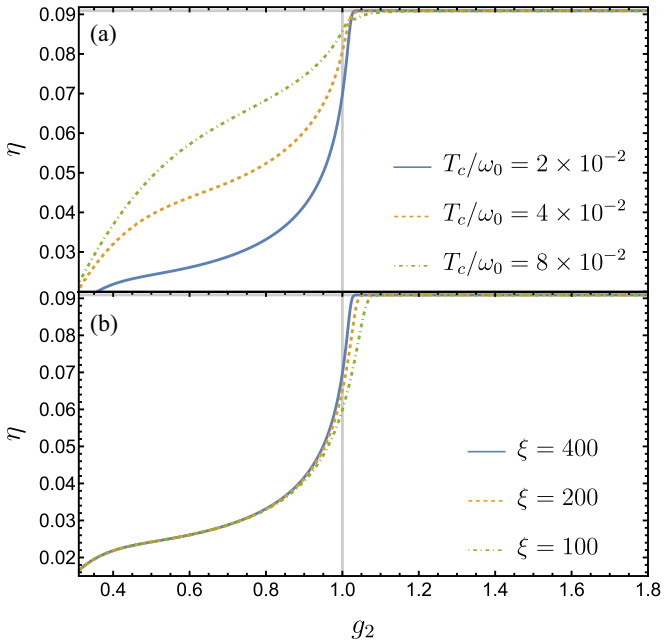


FIG. 2. Numerical evidence for critical Stirling engine of saturating to the Carnot efficiency in the low-temperature limit. (a) The efficiency vs $g_2$ for different temperatures, we set $\xi = 400$. (b) The efficiency vs $g_2$ for different $\xi$, the temperature of the cold reservoir is set to be $T_c/\omega_0 = 2\times10^{-2}$. The vertical gray solid line represents the critical point $g_C = 1$, while the horizontal gray solid line represents the Carnot efficiency. Other parameters: the temperature of the hot reservoir, $T_{\rm h} = 1.1T_{\rm c}$.

One of the key conclusions from this study is that as $g_2$ approaches the critical point, the efficiency of the HE discussed in Sec. II B tends to approach the Carnot efficiency. Additionally, we explore the scenario when $g_2$ crosses the critical point in the low-temperature limit and demonstrate that the efficiency converges to the Carnot efficiency at $g_2 = g_C$. These conclusions find strong support in the numerical results depicted in Figs. 2 and 3.

Figure 2(a) illustrates how the efficiency behaves as the temperature approaches the low-temperature limit. Consistent with theoretical predictions in Sec. III A, the efficiency saturates to the Carnot efficiency at a specific point in the low-temperature cases. We denote this point as $g_{\rm conv}$, i.e., for $g_2 \geqslant g_{\rm conv}$, $\eta_C - \eta = 0$. Unlike theoretical predictions, however, $g_{\rm conv} \neq g_C$, attributed to the finite nature of $\xi$ in numerical simulations compared to the theoretical limit of $\xi \to \infty$. Figure 2(b) demonstrates how the efficiency curve evolves

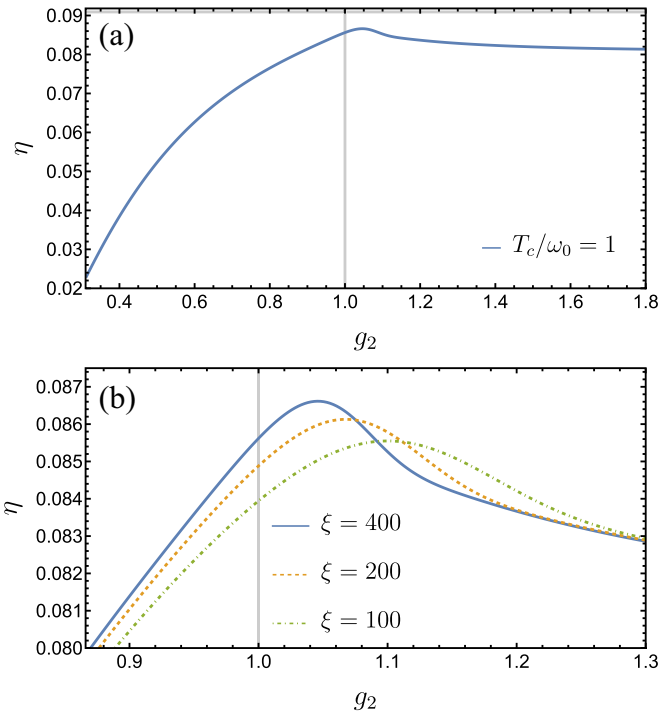


FIG. 3. Efficiency of the critical Stirling engine in finite-temperature cases. (a) The efficiency vs $g_2$ for $T_c/\omega_0 = 1$ and $\xi = 400$. This curve exhibits a maximum value. (b) The efficiency vs $g_2$ for different $\xi$, the cold reservoir temperature is set to be $T_c/\omega_0 = 1$. The vertical gray solid line represents the critical point $g_C = 1$, and the temperature of the hot reservoir $T_h = 1.1T_c$.

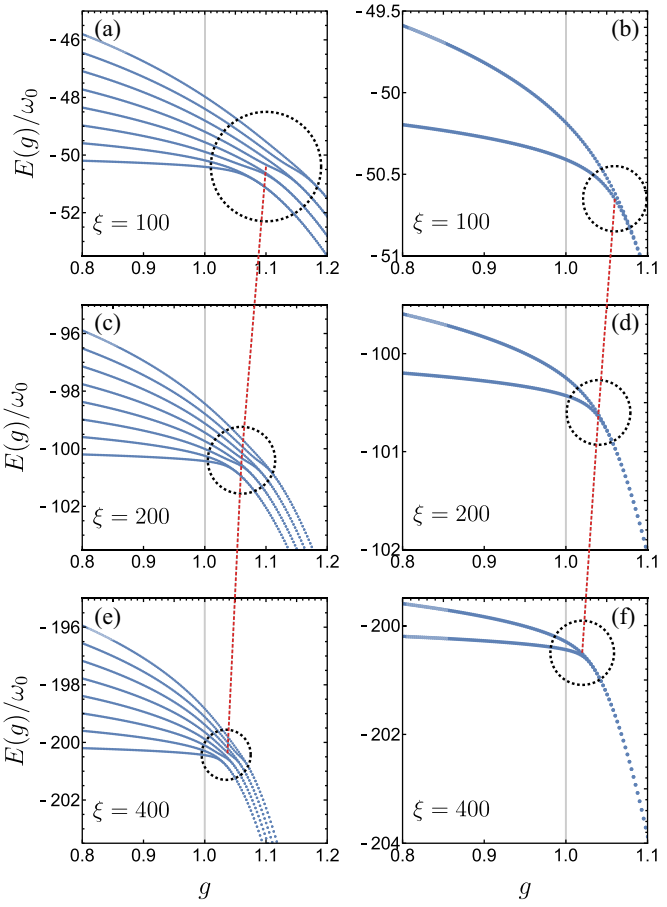


FIG. 4. The lowest eight energies of the QRM vs $g$ with different transition frequencies: (a) $\xi = 100$, (c) $\xi = 200$, and (e) $\xi = 400$. The corresponding lowest two energies are shown in the right column. The vertical gray solid line locates the critical point. In each plot we encompass all degeneracy points with a black dashed circle and connect the centers of these circles in each column with a red dashed line. The trend of the red lines indicates that with increasing $\xi$, all degeneracy points move closer to $g_C$. The size of the circles encompassing all degeneracy points in the left column decreases, suggesting a narrowing of the energy gaps between degenerate levels.

with changing $\xi$. It is noteworthy that $g_{\text{conv}}$ approaches $g_C$ with increasing $\xi$.

Figure 3 shows how the efficiency changes with $g_2$ when the temperature and $\xi$ are both finite. As depicted in Fig. 3(a), the efficiency reaches a maximum. We define $g_m$ as the value of $g_2$ at maximum efficiency for finite $\xi$, expressed as

$$g_m := \text{argmax}[\eta(g_2)], \text{ for finite } \xi. \tag{36}$$

Figure 3(b) illustrates how the efficiency at finite temperatures changes with $\xi$. It is clear that as $\xi$ increases, $g_m$ values approach $g_C$, and the efficiencies approach the Carnot efficiency $\eta_C$. These results indicate that $g_m$ and $\eta$ will achieve $g_C$ and $\eta_C$, respectively, as $\xi \to \infty$. As introduced in Sec. II A, in the limit $\xi \to \infty$, the energy gaps for the normal and superradiant phases are given by Eqs. (7) and (9). Accordingly, the system exhibits infinite degeneracy at $g = g_C$. This infinite degeneracy is a crucial factor leading to the finite-temperature heat engine efficiency approaching the Carnot efficiency as $g_2 \to g_C$. In Fig. 4 we present the lowest eight energy levels of the QRM. It is evident that in the case of finite $\xi$, the energy levels of the QRM also exhibit degeneracy. Moreover, unlike the $\xi \to \infty$ scenario, the degeneracy points differ for distinct pairs of degenerate energy levels, with higher energy levels corresponding to larger values of $g$ at which degeneracy occurs. However, as depicted in the figure, with increasing $\xi$, all degeneracy points approach $g_C$. Simultaneously, the spacing between different degenerate energy levels decreases with increasing $\xi$. These trends in the energy spectrum imply that the energy levels tend to become infinitely degenerate at the critical point as $\xi$ approaches infinity. The deviation of degeneracy points at finite $\xi$ from $g_C$ explains the discrepancies in Figs. 2 and 3 compared to the theoretical analysis with $\xi \to \infty$ in Sec. II A, including deviations in the finite-temperature cases and its asymptotic behavior.

## V. CONCLUSION AND DISCUSSION

In this paper we explore the influence of quantum criticality on the efficiency of a Stirling cycle that utilizes the QRM as its WS. We assume that the effective coupling constant $g$ is the only tunable parameter of the QRM Hamiltonian needed to complete the thermodynamic cycle. The Stirling cycle comprises two isochoric processes with corresponding coupling constants of $g_1$ and $g_2$ such that $g_1 < g_2$. Our results demonstrate that the efficiency approaches the Carnot efficiency when the thermodynamic cycle satisfies the

conditions $g_1 < g_2 \to g_C$. This statement should be understood in an asymptotic sense, namely, it is possible to get as close as one wants to the critical point and hence to the Carnot efficiency. Furthermore, we derive an analytical expression for the efficiency of the quantum Stirling engine when $g_2$ is near the critical point. Our analysis reveals that as $g_2$ approaches the critical point, the asymptotic behavior of a quantum heat engine is characterized by a logarithmic divergence in the denominator. Additionally, we provide a numerical demonstration of our analytical findings, which includes an explicit analysis of the finite-$\xi$ effect.

This study deepens our understanding of how criticality affects the performance of a Stirling heat engine while also advancing our appreciation of criticality. At last, it would be interesting to mention an experimental possibility to realize the criticality of the QRM. It is well known that the occurrence of an superradiant phase transition (SPT) in the QRM cannot be observed in cavity QED due to the presence of a no-go theorem. Recently, although the SPT has not been observed in circuit QED, there have been proposals to utilize a hybrid circuit QED system to circumvent the no-go theorem and achieve a single-photon-triggered SPT [65,66]. Given the experimental challenges encountered in the cavity and circuit QED systems, quantum simulation offers an alternative way for experimentally studying the SPT of the QRM. Notably, the SPT of the standard QRM has been successfully simulated using trapped ions [64] and an NMR system [67], which encourages us to expect that the experimental study on the criticality of the QRM heat engine will come soon.

## ACKNOWLEDGMENTS

This work was supported by the Natural Science Foundation of Guangdong Province (Grant No. 2017B030308003), the Key R&D Program of Guangdong Province (Grant No. 2018B030326001), the Science, Technology and Innovation Commission of Shenzhen Municipality (Grants No. JCYJ20170412152620376, No. JCYJ20170817105046702, and No. KYTDPT20181011104202253), the National Natural Science Foundation of China (Grants No. 12135003, No. 12075025, No. 12047501, No. 11875160, No. U1801661, and No. 11905100), and the Economy, Trade and Information Commission of Shenzhen Municipality (Grant No. 201901161512).

## APPENDIX A: THE CAPACITY FUNCTION $\mathcal{C}(x)$

Given the internal energy in the normal phase in Eq. (10), it can be straightforwardly obtained that

$$\frac{\partial}{\partial T}U(T,g)=\frac{\varepsilon_{\rm np}^2(g)}{T^2}\frac{e^{\varepsilon_{\rm np}(g)/T}}{[e^{\varepsilon_{\rm np}(g)/T}-1]^2}. \tag{A1}$$

Considering the function we defined in the main text,

$$\mathcal{C}(x)\equiv\left(\frac{x}{2}\right)^2\operatorname{csch}^2\frac{x}{2}=\frac{x^2e^x}{(e^x-1)^2}, \tag{A2}$$

we can write the capacity as

$$\frac{\partial}{\partial T}U(T,g)=\mathcal{C}[\varepsilon_{\rm np}(g)/T]. \tag{A3}$$

In the following we will prove that $\mathcal{C}(x)$ is a monotonically decreasing function. The derivative of $\mathcal{C}(x)$ is

$$\frac{d}{dx}\mathcal{C}(x)=-\frac{x}{4}\operatorname{csch}\frac{x}{2}\left(x\cosh\frac{x}{2}-2\sinh\frac{x}{2}\right). \tag{A4}$$

We can see that $x\operatorname{csch}x/2>0$ when $x>0$. The term in the above brackets is also positive when $x>0$, because it equals zero when $x=0$ and is nondecreasing as

$$\frac{d}{dx}\left(x\cosh\frac{x}{2}-2\sinh\frac{x}{2}\right)=\frac{x}{2}\sinh\frac{x}{2}\geqslant 0.$$

As a result, we prove that the derivative of capacity $\mathcal{C}(x)$ is a monotonically decreasing function due to $d\mathcal{C}(x)/dt<0$. In addition, it is simple to demonstrate $\lim_{x\to 0}\mathcal{C}(x)=1$ and $\lim_{x\to\infty}\mathcal{C}(x)=0$. Thus, $\mathcal{C}(x)\in(0,1)$ for $x\in(0,\infty)$.

Next we discuss the heat capacity in the superradiant phase. As we have introduced in Sec. II A, the diagonalized QRM Hamiltonian in the $g>g_C$ regime reads $H_{\rm sp}=\varepsilon_{\rm sp}b^\dagger b-\Omega(g^2+g^{-2})/4$, and combining with Eq. (9), one can get the internal energy in the superradiant phase by the same way Eq. (10) was derived,

$$U_{\rm sp}=\frac{\varepsilon_{\rm sp}}{\exp(\varepsilon_{\rm sp}/T)-1}-\frac{\Omega(g^2+g^{-2})}{4}, \tag{A5}$$

and straightforwardly, we have the heat capacity in the normal phase:

$$\frac{\partial}{\partial T}U_{\rm sp}(T,g)=\frac{\varepsilon_{\rm sp}^2(g)}{T^2}\frac{e^{\varepsilon_{\rm sp}(g)/T}}{[e^{\varepsilon_{\rm sp}(g)/T}-1]^2}. \tag{A6}$$

By the definition in Eq. (A2), the above heat capacity can be rewritten as

$$\frac{\partial}{\partial T}U_{\rm sp}(T,g)=\mathcal{C}[\varepsilon_{\rm sp}(g)/T], \tag{A7}$$

which has the same form as (A3), with the only difference being the replacement of the excitation energy in the normal phase $\varepsilon_{\rm np}$ with the excitation energy in the superradiant phase $\varepsilon_{\rm sp}$. For cases in which $g_2>g_C$, by the same way Eq. (20) was derived, one can obtain a similar inequality as follows:

$$-(T_{\rm h}-T_{\rm c})\mathcal{C}[\varepsilon_{\rm sp}(g_2)/T_{\rm h}]<Q_{\rm BC}<0. \tag{A8}$$

Similarly, the inequality (23) is not available in the regime $g_2>g_C$; instead, the following relation can be derived:

$$-\frac{T_{\rm h}-T_{\rm c}}{T_{\rm c}}\mathcal{C}[\varepsilon_{\rm sp}(g_2)/T_{\rm h}]<S_{\rm BC}<0. \tag{A9}$$

## APPENDIX B: THE EXACT DIAGONALIZATION OF THE QRM

In formulating the numerical results, we first perform numerical diagonalization on the Hamiltonian of the QRM in Eq. (1). In the truncated basis $\{|+,-(N-1)\rangle,|+,-(N-2)\rangle,\ldots,|+,0\rangle,|-,0\rangle,\ldots,|-,N-2\rangle,|-,N-1\rangle\}$, where $|\pm\rangle$ are eigenstates of $\sigma_z$, satisfying $\sigma_z|\pm\rangle=\pm|\pm\rangle$, $\{|n\rangle|n=0,1,2,\ldots,N-1\}$ are Fock states, and the QRM Hamiltonian in Eq. (1) can be written in the following form:

$$H=\begin{pmatrix}H_{++} & H_{+-}\\ H_{-+} & H_{--}\end{pmatrix}, \tag{B1}$$

where

$$H_{\pm\pm} = \begin{pmatrix} \frac{\Omega}{2} & 0 & 0 & \cdots & 0 \\ 0 & \omega_0 \pm \frac{\Omega}{2} & 0 & \ddots & \vdots \\ 0 & 0 & \ddots & \ddots & 0 \\ \vdots & \ddots & \ddots & (N-2)\omega_0 \pm \frac{\Omega}{2} & 0 \\ 0 & \cdots & 0 & 0 & (N-1)\omega_0 \pm \frac{\Omega}{2} \end{pmatrix}, \tag{B2}$$

$$H_{+-} = H_{-+} = \begin{pmatrix} 0 & -\lambda & 0 & \cdots & 0 \\ -\lambda & 0 & \ddots & \ddots & \vdots \\ 0 & \ddots & \ddots & -\lambda\sqrt{N-3} & 0 \\ \vdots & \ddots & -\lambda\sqrt{N-3} & 0 & -\lambda\sqrt{N-2} \\ 0 & \cdots & 0 & -\lambda\sqrt{N-2} & 0 \end{pmatrix}. \tag{B3}$$

By applying exact diagonalization to the above Hamiltonian, we get its eigenvalues $\{E_k | k = 1, 2, \ldots, N\}$.


[1] J. Gemmer, M. Michel, and G. Mahler, *Quantum Thermodynamics* (Springer, New York, 2009).

[2] F. Binder, L. A. Correa, C. Gogolin, J. Anders, and G. Adesso, *Thermodynamics in the Quantum Regime* (Springer, New York, 2018).

[3] H. T. Quan, P. Zhang, and C. P. Sun, Quantum heat engine with multilevel quantum systems, Phys. Rev. E **72**, 056110 (2005).

[4] H. T. Quan, Yu-xi Liu, C. P. Sun, and F. Nori, Quantum thermodynamic cycles and quantum heat engines, Phys. Rev. E **76**, 031105 (2007).

[5] D. Gelbwaser-Klimovsky, W. Niedenzu, and G. Kurizki, in *Thermodynamics of Quantum Systems under Dynamical Control* (Academic Press, New York, 2015), Chap. 12, pp. 329–407.

[6] N. M. Myers, O. Abah, and S. Deffner, Quantum thermodynamic devices: From theoretical proposals to experimental reality, AVS Quantum Sci. **4**, 027101 (2022).

[7] L. M. Cangemi, C. Bhadra, and A. Levy, Quantum engines and refrigerators, arXiv:2302.00726.

[8] M. O. Scully, K. R. Chapin, K. E. Dorfman, M. B. Kim, and A. Svidzinsky, Quantum heat engine power can be increased by noise-induced coherence, Proc. Natl. Acad. Sci. USA **108**, 15097 (2011).

[9] J. Klatzow, J. N. Becker, P. M. Ledingham, C. Weinzetl, K. T. Kaczmarek, D. J. Saunders, J. Nunn, I. A. Walmsley, R. Uzdin, and E. Poem, Experimental demonstration of quantum effects in the operation of microscopic heat engines, Phys. Rev. Lett. **122**, 110601 (2019).

[10] R. Uzdin, Coherence-induced reversibility and collective operation of quantum heat machines via coherence recycling, Phys. Rev. Appl. **6**, 024004 (2016).

[11] K. Korzekwa, M. Lostaglio, J. Oppenheim, and D. Jennings, The extraction of work from quantum coherence, New J. Phys. **18**, 023045 (2016).

[12] P. Kammerlander and J. Anders, Coherence and measurement in quantum thermodynamics, Sci. Rep. **6**, 22174 (2016).

[13] M. Perarnau-Llobet, K. V. Hovhannisyan, M. Huber, P. Skrzypczyk, N. Brunner, and A. Acín, Extractable work from correlations, Phys. Rev. X **5**, 041011 (2015).

[14] W. Ji, Z. Chai, M. Wang, Y. Guo, X. Rong, F. Shi, C. Ren, Y. Wang, and J. Du, Spin quantum heat engine quantified by quantum steering, Phys. Rev. Lett. **128**, 090602 (2022).

[15] D. Gelbwaser-Klimovsky, A. Bylinskii, D. Gangloff, R. Islam, A. Aspuru-Guzik, and V. Vuletic, Single-atom heat machines enabled by energy quantization, Phys. Rev. Lett. **120**, 170601 (2018).

[16] J.-P. Brantut, C. Grenier, J. Meineke, D. Stadler, S. Krinner, C. Kollath, T. Esslinger, and A. Georges, A thermoelectric heat engine with ultracold atoms, Science **342**, 713 (2013).

[17] Y. Zou, Y. Jiang, Y. Mei, X. Guo, and S. Du, Quantum heat engine using electromagnetically induced transparency, Phys. Rev. Lett. **119**, 050602 (2017).

[18] J. Roßnagel, S. T. Dawkins, K. N. Tolazzi, O. Abah, E. Lutz, F. Schmidt-Kaler, and K. Singer, A single-atom heat engine, Science **352**, 325 (2016).

[19] G. Maslennikov, S. Ding, R. Hablützel, J. Gan, A. Roulet, S. Nimmrichter, J. Dai, V. Scarani, and D. Matsukevich, Quantum absorption refrigerator with trapped ions, Nat. Commun. **10**, 202 (2019).

[20] N. Van Horne, D. Yum, T. Dutta, P. Hänggi, J. Gong, D. Poletti, and M. Mukherjee, Single-atom energy-conversion device with a quantum load, npj Quantum Inf. **6**, 37 (2020).

[21] J. Klaers, S. Faelt, A. Imamoglu, and E. Togan, Squeezed thermal reservoirs as a resource for a nanomechanical engine beyond the Carnot limit, Phys. Rev. X **7**, 031044 (2017).

[22] C. Elouard, M. Richard, and A. Auffèves, Reversible work extraction in a hybrid opto-mechanical system, New J. Phys. **17**, 055018 (2015).

[23] M. Brunelli, A. Xuereb, A. Ferraro, G. De Chiara, N. Kiesel, and M. Paternostro, Out-of-equilibrium thermodynamics of quantum optomechanical systems, New J. Phys. **17**, 035016 (2015).

[24] K. Zhang, F. Bariani, and P. Meystre, Quantum optomechanical heat engine, Phys. Rev. Lett. **112**, 150602 (2014).

[25] C. Bergenfeldt, P. Samuelsson, B. Sothmann, C. Flindt, and M. Büttiker, Hybrid microwave-cavity heat engine, Phys. Rev. Lett. **112**, 076803 (2014).

[26] D. M. Kennes, D. Schuricht, and V. Meden, Efficiency and power of a thermoelectric quantum dot device, Europhys. Lett. **102**, 57003 (2013).

[27] R. Sánchez, B. Sothmann, A. N. Jordan, and M. Büttiker, Correlations of heat and charge currents in quantum-dot thermoelectric engines, New J. Phys. **15**, 125001 (2013).

[28] B. Sothmann, R. Sánchez, and A. N. Jordan, Thermoelectric energy harvesting with quantum dots, Nanotechnology **26**, 032001 (2015).

[29] M. Josefsson, A. Svilans, A. M. Burke, E. A. Hoffmann, S. Fahlvik, C. Thelander, M. Leijnse, and H. Linke, A quantum-dot heat engine operating close to the thermodynamic efficiency limits, Nat. Nanotechnol. **13**, 920 (2018).

[30] J. P. S. Peterson, T. B. Batalhão, M. Herrera, A. M. Souza, R. S. Sarthour, I. S. Oliveira, and R. M. Serra, Experimental characterization of a spin quantum heat engine, Phys. Rev. Lett. **123**, 240601 (2019).

[31] Q. Bouton, J. Nettersheim, S. Burgardt, D. Adam, E. Lutz, and A. Widera, A quantum heat engine driven by atomic collisions, Nat. Commun. **12**, 2063 (2021).

[32] K. Ono, S. N. Shevchenko, T. Mori, S. Moriyama, and F. Nori, Analog of a quantum heat engine using a single-spin qubit, Phys. Rev. Lett. **125**, 166802 (2020).

[33] D. von Lindenfels, O. Gräb, C. T. Schmiegelow, V. Kaushal, J. Schulz, M. T. Mitchison, J. Goold, F. Schmidt-Kaler, and U. G. Poschinger, Spin heat engine coupled to a harmonic-oscillator flywheel, Phys. Rev. Lett. **123**, 080602 (2019).

[34] L.-M. Zhao and G.-F. Zhang, Entangled quantum Otto heat engines based on two-spin systems with the Dzyaloshinski-Moriya interaction, Quantum Inf. Process. **16**, 216 (2017).

[35] A. Guthrie, C. D. Satrya, Y.-C. Chang, P. Menczel, F. Nori, and J. P. Pekola, Cooper-pair box coupled to two resonators: An architecture for a quantum refrigerator, Phys. Rev. Appl. **17**, 064022 (2022).

[36] A. Ronzani, B. Karimi, J. Senior, Y.-C. Chang, J. T. Peltonen, C. Chen, and J. P. Pekola, Tunable photonic heat transport in a quantum heat valve, Nat. Phys. **14**, 991 (2018).

[37] J. P. Pekola and I. M. Khaymovich, Thermodynamics in single-electron circuits and superconducting qubits, Annu. Rev. Condens. Matter Phys. **10**, 193 (2019).

[38] Y.-H. Ma, S.-H. Su, and C.-P. Sun, Quantum thermodynamic cycle with quantum phase transition, Phys. Rev. E **96**, 022143 (2017).

[39] M. Campisi and R. Fazio, The power of a critical heat engine, Nat. Commun. **7**, 11895 (2016).

[40] Y.-Y. Chen, G. Watanabe, Y.-C. Yu, X.-W. Guan, and A. del Campo, An interaction-driven many-particle quantum heat engine and its universal behavior, npj Quantum Inf. **5**, 88 (2019).

[41] J. Jaramillo, M. Beau, and A. del Campo, Quantum supremacy of many-particle thermal machines, New J. Phys. **18**, 075019 (2016).

[42] S. W. Kim, T. Sagawa, S. De Liberato, and M. Ueda, Quantum szilard engine, Phys. Rev. Lett. **106**, 070401 (2011).

[43] J. Bengtsson, M. N. Tengstrand, A. Wacker, P. Samuelsson, M. Ueda, H. Linke, and S. M. Reimann, Quantum szilard engine with attractively interacting bosons, Phys. Rev. Lett. **120**, 100601 (2018).

[44] M. Polettini, G. Verley, and M. Esposito, Efficiency statistics at all times: Carnot limit at finite power, Phys. Rev. Lett. **114**, 050601 (2015).

[45] Y. Zheng and D. Poletti, Quantum statistics and the performance of engine cycles, Phys. Rev. E **92**, 012110 (2015).

[46] L. Fusco, M. Paternostro, and G. De Chiara, Work extraction and energy storage in the Dicke model, Phys. Rev. E **94**, 052122 (2016).

[47] M. Fadaie, E. Yunt, and Ö. E. Müstecaplıoğlu, Topological phase transition in quantum-heat-engine cycles, Phys. Rev. E **98**, 052124 (2018).

[48] S. Chand and A. Biswas, Critical-point behavior of a measurement-based quantum heat engine, Phys. Rev. E **98**, 052147 (2018).

[49] P. Abiuso and M. Perarnau-Llobet, Optimal cycles for low-dissipation heat engines, Phys. Rev. Lett. **124**, 110606 (2020).

[50] R. B. S. V. Mukherjee, U. Divakaran, and A. del Campo, Universal finite-time thermodynamics of many-body quantum machines from Kibble-Zurek scaling, Phys. Rev. Res. **2**, 043247 (2020).

[51] T. Fogarty and T. Busch, A many-body heat engine at criticality, Quantum Sci. Technol. **6**, 015003 (2021).

[52] V. Holubec and A. Ryabov, Work and power fluctuations in a critical heat engine, Phys. Rev. E **96**, 030102(R) (2017).

[53] P. Pietzonka and U. Seifert, Universal trade-off between power, efficiency, and constancy in steady-state heat engines, Phys. Rev. Lett. **120**, 190602 (2018).

[54] C. Purkait and A. Biswas, Performance of Heisenberg-coupled spins as quantum Stirling heat machine near quantum critical point, Phys. Lett. A **442**, 128180 (2022).

[55] M.-J. Hwang, R. Puebla, and M. B. Plenio, Quantum phase transition and universal dynamics in the Rabi model, Phys. Rev. Lett. **115**, 180404 (2015).

[56] M. Liu, S. Chesi, Z.-J. Ying, X. Chen, H.-G. Luo, and H.-Q. Lin, Universal scaling and critical exponents of the anisotropic quantum Rabi model, Phys. Rev. Lett. **119**, 220601 (2017).

[57] G. Piccitto, M. Campisi, and D. Rossini, The Ising critical quantum Otto engine, New J. Phys. **24**, 103023 (2022).

[58] F. Altintas, A. Ü. C. Hardal, and Ö. E. Müstecaplıoğlu, Rabi model as a quantum coherent heat engine: From quantum biology to superconducting circuits, Phys. Rev. A **91**, 023816 (2015).

[59] G. Alvarado Barrios, F. J. Peña, F. Albarrán-Arriagada, P. Vargas, and J. C. Retamal, Quantum mechanical engine for the quantum Rabi model, Entropy (Basel) **20**, 767 (2018).

[60] Y. Wang, M. Liu, W.-L. You, S. Chesi, H.-G. Luo, and H.-Q. Lin, Resilience of the superradiant phase against $A^2$ effects in the quantum Rabi dimer, Phys. Rev. A **101**, 063843 (2020).

[61] B. Zohuri, *Physics of Cryogenics: An Ultralow Temperature Phenomenon* (Elsevier Science, 2017).

[62] A. Solfanelli, M. Falsetti, and M. Campisi, Nonadiabatic single-qubit quantum Otto engine, Phys. Rev. B **101**, 054513 (2020).

[63] R. Puebla, M.-J. Hwang, J. Casanova, and M. B. Plenio, Probing the dynamics of a superradiant quantum phase transition with a single trapped ion, Phys. Rev. Lett. **118**, 073001 (2017).

[64] M.-L. Cai, Z.-D. Liu, W.-D. Zhao, Y.-K. Wu, Q.-X. Mei, Y. Jiang, L. He, X. Zhang, Z.-C. Zhou, and L.-M. Duan, Observation of a quantum phase transition in the quantum Rabi model with a single trapped ion, Nat. Commun. **12**, 1126 (2021).

[65] X.-Y. Lü, L.-L. Zheng, G.-L. Zhu, and Y. Wu, Single-photon-triggered quantum phase transition, Phys. Rev. Appl. **9**, 064006 (2018).

[66] X.-Y. Lü, G.-L. Zhu, L.-L. Zheng, and Y. Wu, Entanglement and quantum superposition induced by a single photon, Phys. Rev. A **97**, 033807 (2018).

[67] X. Chen, Z. Wu, M. Jiang, X.-Y. Lü, X. Peng, and J. Du, Experimental quantum simulation of superradiant phase transition beyond no-go theorem via antisqueezing, Nat. Commun. **12**, 6281 (2021).